Encapsulation of functional solvents for improved thermal stability in CO_2 capture applications

Cameron Taylor[1,†], Aidan Klemm[2,†], Luma Al-Mohbobi[1], Jack Bradford[1], Burcu Gurkan[*2], Emily Pentzer[*1,3]

[1]Department of Materials Science & Engineering, Texas A&M University, 3003 TAMU; College Station, TX 77843 (USA)
[2]Department of Chemical and Biomolecular Engineering, Case Western Reserve University, Cleveland, Ohio 44106, Unites States
[3]Department of Chemistry, Texas A&M University, College Station, Texas 77843, USA

[†] Contributed equally

*Corresponding Author: beg23@case.edu ; emilypentzer@tamu.edu

Abstract

Herein we address the efficiency of CO_2 sorption of ionic liquids (IL) with hydrogen bond donors (e.g., glycols) added as viscosity modifiers and the impact of encapsulating them to limit sorbent evaporation. Ethylene glycol, propylene glycol, 1,3-propanediol, and diethylene glycol were added to three different ILs: 1-ethyl-3-methylimidazolium 2-cyanopyrrolide ([EMIM][2-CNpyr]), 1-ethyl-3-methylimidazolium tetrafluoroborate ([EMIM][BF_4]), and 1-butyl-3-methylimidazolium tetrafluoroborate ([BMIM][BF_4]). Incorporation of the glycols decreased viscosity on average 51% compared to bulk IL. After encapsulation of the liquid mixtures using a soft template approach, thermogravimetric analysis revealed reductions in volatility of 36 and 40 % on average compared to the unencapsulated liquid mixtures, based on isotherms at 25 and 55 °C, respectively. The encapsulated mixtures of [EMIM][2-CNpyr]:1,3-propanediol and [EMIM][2-CNpyr]:diethylene glycol exhibited the lowest volatility (0.0019 and 0.0002 mmol/h at 25 °C, respectively) and were further evaluated as CO_2 absorption/desorption materials. Based on capacity determined from breakthrough measurements, [EMIM][2-CNpyr]:1,3-propanediol had lower transport limited absorption rate for CO_2 sorption compared to [EMIM][2-CNpyr]:diethylene glycol with 0.08 and 0.03 mol CO_2/kg sorbent, respectively; however, [EMIM][2-CNpyr]:diethylene glycol capsules exhibited higher absorptions capacity at ~500 ppm CO_2 (0.66 compared to 0.47 mol CO_2/kg sorbent for [EMIM][2-CNpyr]:1,3-propanediol). These results show that multiple glycols can be used to reduce IL viscosity while increasing physisorption sites for CO_2 sorption and encapsulation can be utilized to mitigate evaporation of volatile viscosity modifiers.

Introduction

As atmospheric CO_2 concentrations continue to rise, alternative approaches for negative emissions technologies (NET), such as carbon capture, must be implemented in complement to decarbonization efforts to avoid the average global surface temperature from rising greater than 2 °C by the mid-21st century.[1] One NET approach is direct air capture (DAC), which utilizes chemical reactions and/or physical interactions to sequester CO_2 from the atmosphere. DAC is more energy intensive compared to point source CO_2 capture due to the lower concentration of CO_2 in the atmosphere (~420 ppm versus > 1,000 ppm).[2] To date, DAC approaches have focused on liquid solvents[3] (e.g., aqueous amines), solid sorbents[4] (e.g., metal organic frameworks, MOFs), and pressure driven approaches[5] (e.g., membranes). Current technologies in industrial DAC applications are hindered by low CO_2 sorption rates and capacity, high energy demands for sorbent regeneration, and poor scalability.[6]

Solvent-based chemical DAC technologies typically require strong bases due to the low concentration of CO_2 in the atmosphere. For example, aqueous solutions of NaOH and KOH are common in DAC applications, in addition to amines and amine-functionalized molecules (e.g., amino acids).[3,6] Strong bases typically chemisorb CO_2, for example with a hydroxide anion reacting to form bicarbonate and carbonate anions. Although this can be favorable for the capture of CO_2, desorption is highly endothermic; for example, temperatures of ~ 900 °C are required for $CaCO_3$. Aqueous amines are the main solvent for point-source carbon capture (i.e., flue gas), but are not suitable for DAC because the volatile amines evaporate into the environment when large volumes of airflow are passed over the sorbent. Alternatives to aqueous bases and amines, such as amino acids and ionic liquids (ILs), have decreased regeneration temperatures, typically 70-120 °C.[3,7] Further, ILs have negligible volatility, chemical and thermal stability, and tunability making them attractive candidates for DAC.[7] Conventional ILs, such as 1-butyl-3-methylimidazolium hexafluorophosphate [BMIM][PF_6], primarily rely on physisorption of CO_2 into free molar volume.[8,9] By tailoring the functional moieties, task specific ILs (TSILs) can absorb CO_2 via chemisorption, as well as physisorption,[10] offering a promising alternative to other DAC solvents. For example, the Brenneke group developed the TSIL 1-ethyl-3-methylimidazolium 2-cyanopyrrolide ([EMIM][2-CNpyr]),[11] which the Gurkan group demonstrated its DAC abilities.[12,13] The Gurkan group determined two reaction routes are possible for [EMIM][2-CNpyr] DAC: the anion reversibly reacts with CO_2 to form carbamate, or the cation reacts to form imidazolium-carboxylate.[14] Notably, many TSILs are not economically viable for broad implementation in DAC operations compared to current solvents (e.g., aqueous amines, KOH, etc.) due to higher synthesis costs.[15,16]

Applications of ILs and TSILs are limited by high viscosity, primarily during the absorption of CO_2,[17] which can slow CO_2 absorption rate,[15] thereby making the processing of large volumes of air for CO_2 removal a challenge. TSILs for DAC is further limited as solvent pumping costs increase as viscosity increases. One approach to improve CO_2 absorption rates is mixing TSILs with additives to reduce viscosity.[18,19] These solvent systems can also reduce the quantity of IL required and supply additional CO_2 binding motifs to enhance sorption rate and capacity. For instance, Camper et al. showed that mixing imidazolium-based ILs (e.g., [HMIM][Tf_2N]) with amines (e.g., monoethanolamine) improved CO_2 absorption by at least 20 times compared to neat IL due to an increase in chemisorption capacity.[20] Meanwhile, Nookuea et al. demonstrated that adding a hydrogen bond donor (e.g., monoethanolamine) can reduce the overall viscosity of the mixture.[21] The molecular interactions between ILs and other additives have been studied, suggesting that van der Waals interactions (e.g., hydrogen bonding) reduce the evaporation of the

additive as well as improve CO_2 sorption.[19,22] For example, Lee et al. demonstrated that a mixture of [EMIM][2-CNpyr] and ethylene glycol had improved absorption rate of CO_2 which was attributed to reduced viscosity compared to the bulk IL.[19] The authors also determined that EG aided in CO_2 sorption by protonating the anion and forming a complex with CO_2. Importantly, the higher loading of EG (i.e., IL:EG at 1:3) resulted in noticeable evaporative loss, while lower compositions resulted in thermal stability attributed to Coulombic interactions.

Implementation of ILs for DAC is not limited to traditional solvent-based approaches (i.e., bulk liquids), and in complement can be used in various composite structures such as membranes (e.g., polymer-IL, supported IL membranes, and cross-linked gels),[23–25] IL-impregnation in porous structures (e.g., silica),[26–29] and microencapsulation.[14,30–35] Of these composite structures, encapsulation is perhaps the most scalable and most flexible to different compositions. Three main approaches can be used to encapsulate ILs: microfluidics, [36] hard template approach,[37] or soft template approach, of which the soft template approach is the most common. Here, a shell is grown around a droplet of the desired core, typically relying on an emulsion with liquid droplets stabilized by surfactants. The encapsulation of different types of ILs have been studied for post-combustion capture of CO_2 and for DAC. For example, Bernard et al. encapsulated imidazolium based fluorinated ILs from an emulsion, which leads to less uniformity in size distribution.[38] The Pentzer Group has meticulously worked at encapsulating a variety of ILs utilizing the soft template approach stabilized with modified graphene oxide[39–41] with a wide range of applications such as toxin removal,[42–44] CO_2 capture,[14,45,46] protecting phase change materials,[47] and utilizing dynamic chemistry for payload release.[48–50] The Gurkan group has done significant work with developing different deep eutectic solvents, such a choline-based eutectic solvents for CO_2 sorption,[51] and researching the kinetics and intermolecular interactions of the TSILs for CO_2 sorption.[13,52] In collaboration between the two groups, the versatility of the encapsulation techniques enable the applicability of more volatile additives for CO_2 sorbents by having the shell act as a barrier to the solvent while being CO_2 permeable. Currently, there are very limited studies on the role different glycols have for CO_2 sorption and modifying IL viscosity,[53–55] while limited studies have been done on quantifying how well encapsulation can reduce evaporation of volatile compounds (e.g., glycols).[56]

Herein, we demonstrate that glycol-based hydrogen bond donor (HBD) additives can be used to decrease the viscosity of ILs by ~51 % and that the volatility of the glycols can be reduced by 36 and 40% at temperature of 25 and 55 °C, respectively, compared to pure glycols. Further reductions in volatility can be achieved by encapsulating these liquid mixtures with a reduction of 40 and 43% at 25 and 55 °C, respectively, compared to pure glycols. We further demonstrate that encapsulation enhances CO_2 sorption rates of the IL:glycol mixtures, with [EMIM][2-CNpyr]:DEG having the fastest uptake rate compared to [EMIM][2-CNpyr]:1,3-P. The use of DEG and 1,3-P as viscosity modifiers increased the CO_2 capacity by a factor of 3 and 4, respectively. Ethylene glycol (EG), propylene glycol (PG), 1,3-propanediol (1,3-P), and diethylene glycol (DEG) are used as the HBDs and both ILs ([EMIM][BF_4], and [BMIM][BF_4]) and TSIL ([EMIM][2-CNpyr]). This study demonstrates that encapsulating the mixtures using a soft-template microencapsulation approach, the core volatility loss was further minimized with the least volatile samples ([EMIM][2-CNpyr]:1,3-P and [EMIM][2-CNpyr]:DEG) studied for CO_2 sorption applications. With the use of viscosity modifiers and encapsulation, more expensive viscous reactive chemicals (e.g., TSILs) can be more widely utilized in a variety of industries such as wastewater treatment, pharmaceuticals, and consumer goods.

Methods

Materials: The IL 1-ethyl-3-methylimidazolium 2-cyanopyrrolide ([EMIM][2-CNpyr]) with a purity of >95 % was synthesized as previously reported.[14] 1-Ethyl-3-methylimidazolium tetrafluoroborate ([EMIM][BF_4]) (>98 %) and 1-butyl-3-methylimidazolium tetrafluoroborate ([BMIM][BF_4]) (>98 %) were purchased from Iolitec and were dried at 80 °C under reduced pressure for 72 h; [EMIM][2-CNpyr] was dried under reduced pressure at 70 °C for 72 h to avoid thermal decomposition. All other materials were used as received. Graphite flakes, propylamine, potassium permanganate, 4,4′-diaminodiphenylmethane (DAPM), hexamethylene diisocyanate (HDI), diethylene glycol (DEG), 1,3-propanediol (1,3-P), and sulfuric acid (95-98%) were purchased from Sigma-Aldrich. Hexanes, hydrogen peroxide (35 wt% in water), and toluene were purchased from Fisher Scientific. Additionally, n-octane (Oakwood Chemical), ethylene glycol (EG, from Acros Organics), propylene glycol (PG, from TCI), and *N*,*N*-dimethylformamide (DMF, from Alfa Aesar) were all purchased and used as received. Nitrogen gas (Ultra High Purity) and carbon dioxide gas (Bone Dry) were purchased from Airgas.

Instrumentation: Mixture composition and capsule core loading were characterized by nuclear magnetic resonance (NMR) spectroscopy in DSMO-d6 using a Bruker Avance NEO 400 mHz NMR spectrometer. Centrifugation was conducted using a ThermoScientific Sorvall ST 8 centrifuge. Bath ultrasonication was done with a Fisherbrand CPX3800 5.7 L Ultrasonic Bath. Emulsification was done using a BioSpec hand-held homogenizer model 985370. The capsule morphology was analyzed using scanning electron microscopy (Tescan Vega SEM) at a voltage of 10-20 kV; prior to characterization, the sample was sputter-coated with 10 nm of Au (Cressington 108 Sputter Coater). Fourier transform infrared (FTIR) spectroscopy was performed on a JASCO FT/IR-4600 using a diamond coated ZnSe crystal in ATR mode. Thermogravimetric analysis (TGA) was performed on a TA instruments TGA 5500 equipped with a TA Instruments Blending Gas Delivery Module under N_2 and bone-dry CO_2. Viscosity measurements were performed using an Anton Paar MCR-302 rotational rheometer with an Anton Paar 25 mm 0.5 degree cone CP25-0.5 top plate and an Anton Paar 24.986 mm parallel plate. The density of the mixtures was collected using an Anton Paar vibrating U-tube density meter (DMA 4500M) with an accuracy of 0.00005 g/cm3.

IL:glycol Mixture Preparation and Characterization: Mixtures of IL and glycols were prepared with molar ratios of 1:2, and confirmed by ^{1}H NMR spectroscopy using DMSO-d6 as the solvent.

Synthesis of Graphene Oxide (GO): GO nanosheets were synthesized using a modified Hummer's method, as previously reported.[57] Briefly, graphite flakes (3 g) were dispersed in concentrated H_2SO_4 (400 mL) at room temperature. $KMnO_4$ (3 g) was slowly added, and after complete addition the mixture was stirred at room temperature for 24 h; this was repeated 3 times for a total addition of 12 g of $KMnO_4$. Then, after stirring a total of 72 h, the reaction was quenched by adding the solution into three Erlenmeyer flasks each containing ~750 mL of ice water. Dropwise addition of H_2O_2 to the stirred solution was continued until the color turned from pink to brown, indicating excess $KMnO_4$ was consumed. The yellow-brown GO was isolated by centrifugation and subsequent washing of the pellet with isopropanol, each time discarding the supernatant and repeating until the supernatant was neutral by a Litmus test. The GO was then dried overnight under reduced pressure at room temperature, thereafter, blended to a fine powder. The powder was stored in a refrigerator, sealed with parafilm.

Synthesis of Alkylated GO (C_{18}-GO): C_{18}-GO was synthesized following a method previously reported.[39] GO (100 mg) was dispersed in DMF (40 mL) via sonication until no visible aggregates were observed. Meanwhile, octadecylamine (900 mg) was dissolved in DMF (60 mL) by gently heating to 60 °C in a 250 mL round bottom flask (rbf). The GO solution was added to the rbf and the resulting mixture stirred at 55 °C for ~5 minutes. The sample was then centrifuged, and supernatant discarded. The pellet was suspended in toluene (40 mL) via sonication. In a separate rbf, octadecylamine (2.7 g) was dissolved in toluene (60 mL) while stirring at 60 °C. Once the octadecylamine was dissolved, the GO dispersion was added, and the mixture stirred at 55 °C overnight. Thereafter, a dark brown precipitate was isolated via centrifugation, washed with octane (2 x 25 mL, discarding the supernatant each time) and dried under reduced pressure at ambient temperature. When ready to use, ~100 mg of C_{18}-GO was dispersed in 1:1 v/v mixture of octane (25 mL) and heavy mineral oil (25 mL), resulting in a C_{18}-GO concentration of 2 mg/mL.

Synthesis and Characterization of Microcapsules: Based a previously reported method,[40] capsules were synthesized by interfacial polymerization in an emulsion (i.e., a soft template approach). As an example, take the preparation of capsules with a core of pure EG. First, DAPM (0.66 mmol, 130.8 mg) was dissolved in 0.5 mL EG in a 20 mL scintillation vial via sonication. Then, C_{18}-GO in octane/mineral oil (2.5 mL of a 2 mg/mL solution) was added to the EG/DAPM solution and emulsified by 3 cycles of shear mixing (20 s on, 15 s off), which produced an emulsion with droplets of EG/DAPM in a continuous phase of octane and mineral oil. The prepared emulsion was diluted with octane (1 mL). In a separate vial, HDI (0.86 mmol, 137.8 µL) was mixed with octane (1.25 mL) and this solution was added dropwise to the emulsion with swirling the vial by hand. The system was left unagitated at ambient temperature for 72 h, then the capsules were isolated via gravity filtration and washed with hexanes (~100 mL) then dispersed in hexanes (100 mL). Residual isocyanate groups were quenched by adding propylamine (2 mL) to the dispersion and allowing the system to rest for 1-2 h. Finally, the capsules were isolated via gravity filtration and washed with hexanes until pH of effluent is about neutral to verify propylamine removal (~300 mL hexanes). The capsules were air dried for an hour. A similar procedure was used for all capsules, with the discontinuous phase being ILs, glycols, or IL/glycol mixtures. The amount of monomer was consistent across all the samples, excluding the [EMIM][2-CNpyr] capsules for which a second additional HDI was used (0.43 mmol), with a total loading of 1.29 mmol HDI.

The loading of the core liquid in the capsules was determined by extraction of the core using DSMO-d6 and mesitylene standard, and characterization by ^{1}H NMR, as previously reported.[39] Capsules (~20 mg) were weighed in a glass vial and then a 0.038 M mesitylene in DMSO-d6 solution (1 mL) was added. The sample was sonicated for ~3 min to extract the core liquid and then passed through a PTFE syringe filter to separate the solid capsule shell. Relative integration of the ^{1}H NMR signals due to mesitylene and the IL, glycol, or IL and glycol was used to determine the wt% of the core in the capsule (Figure S1). Capsule sizing was done using ImageJ and SEM images with 100-500 capsules per sample.

Evaporation Rate Measurements:
Evaporation rate studies were determined using thermogravimetric analysis (TGA) under an inert N_2 environment. As an example, bulk EG (20 µL) was spread on a tared, flame-cleaned high temperature platinum TGA pan. A 1 h isotherm under N_2 (flow rate of 25 mL/min) was conducted at 25 °C, monitoring the mass. The sample pan was cleaned and a fresh sample of EG (20 µL) was

added and a 1 h isotherm under N_2 (flow rate of 25 mL/min) at 55 °C was collected. A similar procedure was used on all unencapsulated pure glycols, pure ILs, and IL/glycol mixtures. Samples containing 1,3-P and DEG were pretreatment at 55 °C under N_2 (flow rate of 25 mL/min) for 5 min to desorb any volatiles resulting in a stable mass loss at 25 °C.

The evaporation rates of the encapsulated liquids were determined using the method described above. To compare capsules to bulk samples, the molar quantities of the liquids were held constant by using the core wt% loading of the capsules. For example, 20 µL of bulk EG has 0.358 mmol of EG and the capsules of EG had a measured core loading of 60 ± 3 wt% EG. Therefore, the amount of EG capsules used was 37 mg, using:

$$X \text{ mg of capsules} = \frac{(\text{mmol of bulk liquid})(\text{molar mass of liquid})}{\text{core loading wt\%}} \quad (1)$$

The thermal stability of the encapsulated and unencapsulated samples were determined using TGA with heating ramped from ambient temperature to 500 °C by 10 °C/min under N_2 (25 mL/min) (Figure S2).

CO_2 Sorption Studies. The IL:glycol mixtures with the lowest evaporation rates (i.e., [EMIM][2-CNpyr]:1,3-P and [EMIM][2-CNpyr]:DEG) were evaluated for CO_2 sorption utilizing both thermogravimetric and breakthrough techniques.

Thermogravimetric CO_2 sorption studies were conducted using TGA with flowrates of both CO_2 and N_2 at 25 mL/min. On a clean platinum TGA pan, ~10 mg of capsules was loaded. The capsules were pretreated to remove any absorbed gases and moisture at 55 °C under N_2 (25 mL/min) until the mass of the sample exhibited a similar linear mass loss determined from the evaporation studies, as previously determined. Then, the sample was cooled from 55 °C to 25 °C at a rate of 10 °C/min and a baseline mass was established. Then, N_2 was switched to CO_2 (25 mL/min). The mass of the sample increased steadily until a plateau was reached; then, for desorption, CO_2 was replaced with N_2 (25 mL/min) and the temperature was increased to 55 °C (10 °C/min). Decrease in mass was observed and then stabilized at approximately the baseline established with the pretreatment. This CO_2 sorption-desorption cycle was completed 10 times for both capsule samples.

Breakthrough experiments were performed following a previously described procedure.[14] Briefly, capsules (0.25 ± 0.01 g) were lightly packed into a 0.305" inner diameter column, with care taken not to break the capsules. A mixture of 500 ± 5 ppm CO_2 in N_2 (Airgas custom mixture) was fed to the column at 20 standard cm^3/min (sccm) utilizing a mass flow controller (Brooks i5850, 0-200 sccm) and the effluent gas was analyzed by an IR gas sensor. A bypass was used to calibrate the infrared gas analyzer (SBA-5, PP Systems, Inc.) and the gas feed composition was measured. After 1 minute, the feed gas was diverted to the sample column, and the effluent CO_2 concentration was measured over time. The experiment was stopped when the concentration of CO_2 in the effluent reached the feed concentration of 500 ± 5 ppm. Capacity analysis was performed by integrating the breakthrough curve and using the following equation:

$$z = \frac{\int_0^t (C_0 - C)dt * F}{W * \hat{V}_{STP}} \quad (2)$$

where z is the CO_2 loading (mmol CO_2 / g sorbent). C_0 is the dimensionless feed CO_2 composition (concentration in ppm * 10^6), C is the dimensionless effluent CO_2 composition, t is time (min), F

is the total mass flowrate of the feed gas (sccm), W is the weight of the sample (g), and $\hat{V}_{STP}$ is the molar volume of CO_2 at STP (22.4 scc CO_2 / mmol CO_2, assuming ideal gas law in dilute conditions). Breakthrough time (t_{BT}) and pseudoequilibrium time (t_{PE}) are defined as the time at which the effluent concentration reached 25 ppm CO_2 (5% of the feed concentration) and 490 ppm (97.5% of the feed concentration), respectively.

Results and Discussion

Materials Selection, Preparation, and Characterization. Four different glycols were used as viscosity modifiers for three different ILs, each chosen for their commercial availability or ease of accessibility, giving twelve IL:glycol compositions, each prepared using a 1:2 molar ratio of IL to glycol, chosen based on prior studies.[19,58] Two generic ILs ([EMIM][BF_4] and [BMIM][BF_4]) and one TSIL ([EMIM][2-CNpyr]) were chosen. The generic [EMIM][BF_4] and [BMIM][BF_4] absorb CO_2 via physisorption into free volume and differ by the length of one alkyl chain on the imidazolium cation resulting in a difference in viscosities.[25] Recall, [EMIM][2-CNpyr] undergoes chemisorption by reaction of CO_2 via 4 possible routes, as stated earlier.[14,19,59,60] The four glycols were chosen as low-cost and non-corrosive viscosity modifiers with the ability to hydrogen bond through their hydroxyl groups: EG, PG, 1,3-P, and DEG. Thus, all mixtures were homogenous at room temperature, apart from [EMIM][BF_4]:1,3-P and [BMIM][BF_4]:1,3-P which phase separated at room temperature, but form a homogenous solution at 29 °C and 26 °C, respectively.

Figure 1 shows the viscosity of the pure ILs, pure glycols, and their mixtures at 25 °C (with exception for [EMIM][BF_4]:1,3-P and [BMIM][BF_4]:1,3-P which were recorded at 40 °C). The viscosity of the pure ILs were: 75.3 ± 2.1 for [EMIM][2-CNpyr], 21.6 ± 6.2 for [EMIM][BF_4], and 73.0 ± 8.5 for [BMIM][BF_4]. Despite having the same cation, [EMIM][2-CNpyr] and [EMIM][BF_4] have significantly different viscosities. Interestingly, the viscosities of [EMIM][2-CNpyr] and [BMIM][[BF_4] were similar, yet [BMIM][BF_4] had a more significant viscosity reduction with the addition of the glycol modifiers. All IL:glycol mixtures had decreased viscosity compared to the pure ILs, with [EMIM][BF_4] and [BMIM][BF_4] mixtures also having a lower viscosity than the pure glycols. In contrast, [EMIM][2-CNpyr] mixtures were more viscous compared to the corresponding pure glycols. The water content of the mixtures was measured to be between 1876 to 7629 ppm, with EG mixtures having the highest water content (7290 – 7629 ppm) with the other mixtures having a lower water content: PG (2114 – 2241 ppm), 1,3-P (2870 – 3860 ppm), and DEG (1876 – 2704 ppm). All water content data can be found in **Table S1**.

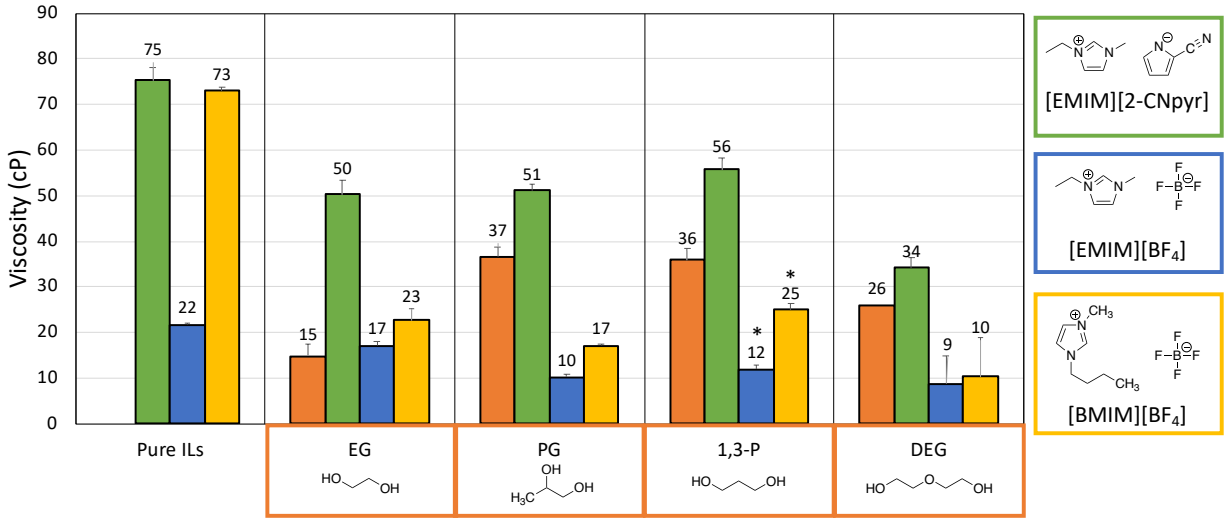

Figure 1: Viscosity of pure ILs and their mixtures for [EMIM][2-CNpyr] (green), [EMIM][BF_4] (blue), [BMIM][BF_4] (yellow), and pure glycols (orange). Data collected at 25 °C except samples marked with an "*" which were taken at 40 °C.

To further examine the molecular interactions of the mixture, excess molar volume was calculated using eq 3:

$$V_m^E = \frac{x_1M_1+x_2M_2}{\rho_{mix}} - \frac{x_1M_1}{\rho_1} - \frac{x_2M_2}{\rho_2} \quad (3)$$

Where ρ is density, x is mole fraction, and M is molar mass. The excess molar volume had negative values for all [EMIM][2-CNpyr]-glycol mixtures, suggesting that hydrogen bond networks formed between the IL and the glycol, thereby resulting in a closer packing of the molecules and higher viscosity.[61] On the other hand, [EMIM][BF_4]- and [BMIM][BF_4]-glycol mixtures had positive excess molar volumes, indicating that the constituent species are not strongly interacting, resulting in lower viscosities. Although the analysis of the mixtures of [EMIM][BF_4] and [BMIM][BF_4] with 1,3-P used the densities at 40 °C, the excess molar volume is still very large and positive (3.9 and 2.1 mL/mol, respectively). These large positive values suggest poor molecular interactions, which is reasonable due to the mixture phase separating at 25 °C. The excess molar volume results have an indirect correlation with the mixture viscosities: as hydrogen bond networks form, molecules are more tightly packed resulting in higher viscosity.

Encapsulation of the pure ILs, pure glycols, and their mixtures was done using a soft-template approach. Briefly, the liquid for the core was shear mixed with an octane/mineral oil dispersion of C_{18}-GO nanosheets (see experimental for details) to form a nanosheet-stabilized Pickering emulsion (**Figure 2A**). By pre-loading the droplet with 4,4′-diaminodiphenylmethane (DAPM) and adding hexamethylene diisocyanate (HDI) into the octane phase of the emulsion, A2+B2 step growth interfacial polymerization of the diamine and diisocyanate yielded a polyurea capsule shell around the droplet (**Figure 2B** and **2C**). The capsules were isolated by gravity filtration then residual isocyanate groups were quenched with propyl amine. The capsules were air dried for 1 h, yielding solid capsules in gram scale (**Figure 2D**); emulsion droplets were slightly smaller than the corresponding capsules, assumedly due to the polymer shell formation around the droplet (i.e., polymerization took place in the outer part of the droplet).

Images of all emulsions and capsules are shown in **Figure S3** and **Figure S4**, respectively, and illustrate spherical emulsion droplets and capsules tens of microns in diameter. The size distribution for each capsule system was evaluated utilizing SEM images and ImageJ analysis of 100-500 capsules per sample (**Table S1**). Overall, the average diameter sizes of the capsules with [EMIM][BF_4] mixtures had the smallest average diameter (23 ± 9 µm), [BMIM][BF_4] mixtures had an average of 42 ± 20 µm, and capsules of [EMIM][2-CNpyr] mixtures had the largest average diameter (52 ± 15 µm). The largest capsules were pure DEG and [EMIM][2-CNpyr]:DEG, 70 ± 29 µm and 70 ± 16 µm, respectively.

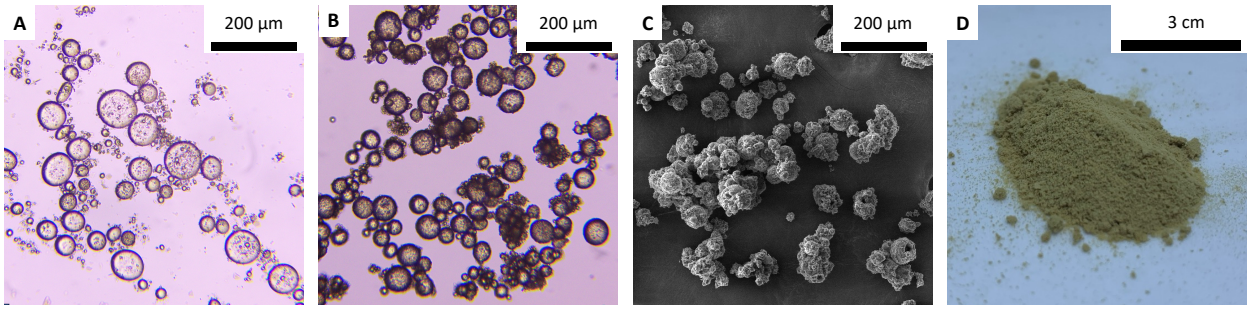

Figure 2. Images of the [EMIM][2-CNpyr]:1,3-P emulsion and capsules: A) Optical microscopy image of emulsion showing discrete IL:glycol droplets in a mineral oil/octane continuous phase, B) Optical microscopy image of capsules before isolation with visible polyurea shell formation, C) SEM image of isolated capsules, D) Photograph of isolated capsules post air-drying for 1 h.

The core loading wt% of the capsules was determined by extracting the core liquid using a deuterated solvent containing an internal standard and characterization of the liquid by ^{1}H NMR spectroscopy (a representative spectrum is shown in Figure S1). The spectra were analyzed by integrating signals from each constituent molecule present and comparing to the internal standard. The average core wt% across all samples was 52 ± 2 wt%. For example, capsules of [EMIM][BF_4] and its mixtures had an average loading of at 62 ± 1 wt% whereas capsules of [BMIM][BF_4] and its mixtures had an average loading of 60 ± 1 wt%. However, capsules of [EMIM][2-CNpyr] and its mixtures had the lowest average loading of 31 ± 2 wt%, which may be due to the thicker shell (i.e., to prepare isolable capsules additional monomer was used). A negative correlation was observed between the core viscosity and loading. Capsules with higher viscosity cores resulted in a lower wt% of core material, for example, [EMIM][2-CNpyr] (viscosity of 75.3 ± 2.1 cP) had a core loading of 25 ± 1.8 wt%. Meanwhile, [EMIM][BF_4]:EG (viscosity of 10.3 ± 0.7 cP) had a core loading of 63 ± 0.9 wt%.

Volatility Measurements. Volatility of the bulk and encapsulated liquids was examined by determining the evaporation rates using thermogravimetric analysis (TGA). First, isotherms under N_2-feed were established for all systems at 25 °C and 55 °C, using a fresh sample for each. Notably, the pure ILs have no detectable evaporation rate at either temperature after initial minimal weight loss by desorption of, e.g., water vapor or gases, as previously documented (Figure S6).[14,62] The evaporation rates for the glycols and IL/glycol mixtures were established by taking the slope of the last 10 min of the 1 h isotherm, with the assumption that evaporation was due to loss of the glycol component. The evaporation rate expressed in mmol/h can be found in **Table 1** and graphically in **Figure 3**.

Table 1: Evaporation rates of bulk and encapsulated pure glycols and their mixtures at 25 and 55 °C, with the values at 55 °C in parenthesis.

Evaporation Rates (mmol/h 1×10^{-2})								
25 °C (55 °C)	**Pure Glycols**		**[EMIM][2-CNpyr]**		**[BMIM][BF_4]**		**[EMIM][BF_4]**	
	Bulk	**Caps**	**Bulk**	**Caps**	**Bulk**	**Caps**	**Bulk**	**Caps**
EG	1.43 (5.20)	1.01 (2.25)	0.40 (2.02)	0.28 (0.71)	0.48 (3.58)	0.37 (2.59)	0.58 (4.00)	0.49 (1.64)
PG	0.83 (6.99)	0.53 (5.28)	0.28 (2.38)	0.18 (1.61)	0.69 (5.53)	0.33 (2.64)	0.76 (5.01)	0.33 (1.61)
1,3-P	0.45 (1.57)	0.15 (0.68)	0.20 (0.69)	0.19 (0.41)	0.17 (1.21)	0.11 (0.84)	0.17 (1.40)	0.11 (0.60)
DEG	0.05 (0.46)	0.05 (0.46)	0.05 (0.19)	0.02 (0.08)	0.06 (0.29)	0.02 (0.12)	0.10 (0.34)	0.04 (0.14)

The evaporation rates of the bulk glycols and their mixtures with ILs at 25 °C had a trend dependent on the glycol, with the evaporation rate of EG > PG > 1,3-P > DEG, which correlates with previous reports of the bulk glycols.[63–65] Perhaps surprisingly, the evaporation rates of the IL/glycol mixtures were also dependent on the identity of the IL, with volatility trending as [EMIM][BF_4] > [BMIM][BF_4] > [EMIM][2-CNpyr]. In all cases, addition of the IL to the glycol decreased the volatility of the glycol, which can be attributed to favorable interactions between the components, e.g., ion-dipole and dipole-dipole interactions.[66] The evaporation rates of bulk [EMIM][BF_4]- and [BMIM][BF_4]-glycol mixtures were somewhat similar to each other (0.10 – 0.76 mmol/h and 0.06 – 0.69 mmol/h, respectively), whereas bulk [EMIM][2-CNpyr]-glycol mixtures had the highest viscosity hence presents more ionic interactions and therefore, these results are consistent with the above discussed results (0.05 – 0.40 mmol/h). Diffusion limitations of the glycol in the IL may contribute to lower evaporation rates in mixtures compared to the pure glycol, as diffusion of glycols to the surface is slowed by the hydrogen bonding network. Notably, both DEG and IL-DEG mixtures had similar evaporation rates at 25 °C (0.05 – 0.10 mmol/h). Now, examining the isotherm at 55 °C, the bulk material exhibited a similar trend that was seen at the 25 °C isotherm, however, PG has the overall highest evaporation rate: PG > EG > 1,3-P > DEG. In general, the mixture volatility was primarily dependent on the IL where [EMIM][BF_4] (0.34 – 5.01 mmol/h) > [BMIM][BF_4] (0.29 – 5.53 mmol/h) > [EMIM][2-CNpyr] (0.19 – 2.38 mmol/h,) , with the noticeable exception of [BMIM][BF_4]:PG having a higher evaporation rate compared to the other IL:PG mixtures at 5.53 mmol/h.

The encapsulated glycols and their IL mixtures had a much lower evaporation rate compared to the bulk analog. At 25 °C the general evaporation rate trend was EG > PG > 1,3-P > DEG. Contrary to the bulk analog, the IL evaporation rate trend was different for the capsules. For the IL:EG mixtures, the evaporation rates were [EMIM][BF_4] > [BMIM][BF_4] > [EMIM][2-CNpyr]. However, IL:PG and IL:1,3-P had evaporation rates of [EMIM][BF_4] = [BMIM][BF_4] > [EMIM][2-CNpyr] and [EMIM][2-CNpyr] > [EMIM][BF_4] = [BMIM][BF_4], respectively. Lastly, IL:DEG had an evaporation rate trend of [EMIM][BF_4] > [BMIM][BF_4] = [EMIM][2-CNpyr]. To be clear, [EMIM][2-CNpyr]:glycol mixtures tend to have the lowest evaporation rates, however, [EMIM][2-CNpyr]:1,3-P had a higher evaporation rate compared to pure 1,3-P and the other IL:1,3-P mixtures. This is likely due to poor capsule formation which led to core leakage during

the handling of the capsules. Examining the 55 °C isotherm for the capsules, the pure encapsulated glycols had a general evaporation rate trend of PG > EG > 1,3-P > DEG. Interestingly, the encapsulated IL mixture evaporation rate trend was different at 55 °C compared to 25 °C where [BMIM][BF_4] > [EMIM][BF_4] > [EMIM][2-CNpyr]. The only exception was with IL:DEG with the trend being [EMIM][BF_4] > [BMIM][BF_4] > [EMIM][2-CNpyr].

Comparing the overall bulk and encapsulated evaporation rates of the pure glycols to the IL:glycol mixtures, the mixtures exhibited a decrease in evaporation by an average of 36 and 40 % based on the isotherms at 25 and 55 °C, respectively. [EMIM][2-CNpyr]:glycol mixture evaporation rates decreased by 45 and 62 % compared to the pure glycol evaporation rates at 25 and 55 °C, respectively. The mixtures containing DEG had the largest evaporation decrease with encapsulation by 47 and 72 % at 25 and 55 °C, respectively. These results suggest that introducing a glycol as a viscosity modifier can reduce the viscosity of the IL while lowering the volatility of the glycol which can increase the working life of these encapsulated systems. Thus, capsules of [EMIM][2-CNpyr]:1,3-P and [EMIM][2-CNpyr]:DEG were selected for CO_2 sorption and thermal desorption studies because they had the lowest evaporation rates of all systems evaluated.

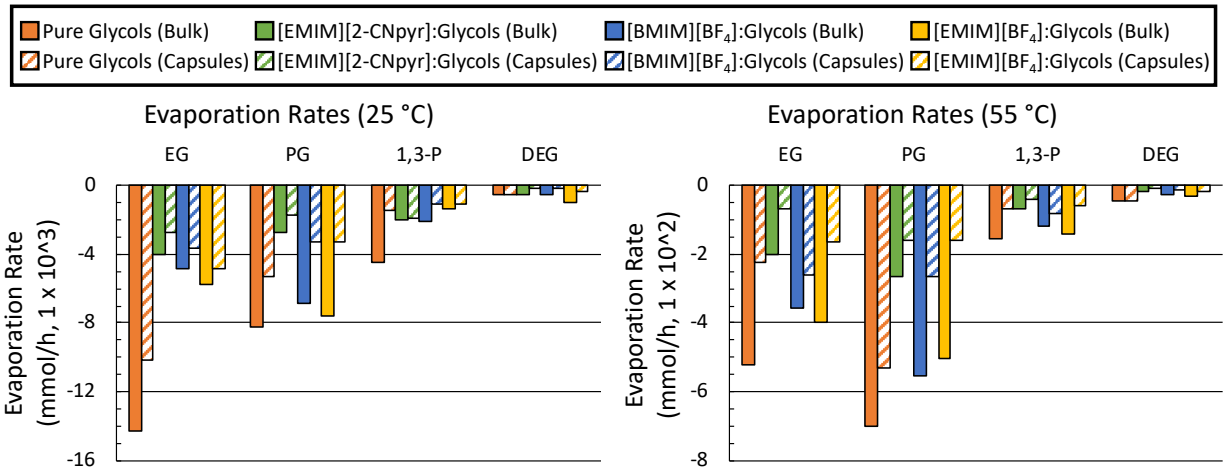

Figure 3. Evaporation rates of bulk liquids (solid) and encapsulated liquids (striped) at (A) 25 °C and (B) 55 °C all under a pure N_2 environment using TGA. The slope of the last 10 minutes of the isotherms was determined and converted to mmol/h. To enable comparison between a bulk and encapsulated sample, the molar quantity was held constant for each of the experiments.

CO_2 Uptake Experiments. CO_2 sorption for the encapsulated IL-glycols was performed at 25 °C with a pure CO_2-gas stream and thermal desorption was performed at 55 °C under a N_2 gas stream, performing ten sorption-desorption cycles. The first cycle was used to condition the material and determine the sorption and desorption times. **Figure 4** shows the sorption/desorption cycles for [EMIM][2-CNpyr]:1,3-P and [EMIM][2-CNpyr]:DEG capsules. For both systems, a slight decrease in capacity is observed with each cycle (**Figure 4A, 4B**), this may be attributed to residual CO_2 that did not desorb completely out of the capsule core. Additionally, some evaporation of the core liquid likely occurred, which is supported by a decrease in the baseline mass with each cycle (**Figure 4C, 4D**); the average rate loss of sample mass was determined to be 3.6×10^{-4} and 1.8×10^{-4} mmol/h for [EMIM][2-CNpyr]:1,3-P and [EMIM][2-CNpyr]:DEG, respectively. This was lower than expected based on the evaporation rate of the capsules under a 1 h isotherm, as discussed above. After the first sorption-desorption cycle, the subsequent cycles had consistent

sample mass loss per cycle (0.024 ± 0.002 and 0.024 ± 0.003 mg for [EMIM][2-CNpyr]:1,3-P and [EMIM][2-CNpyr]:DEG, respectively).

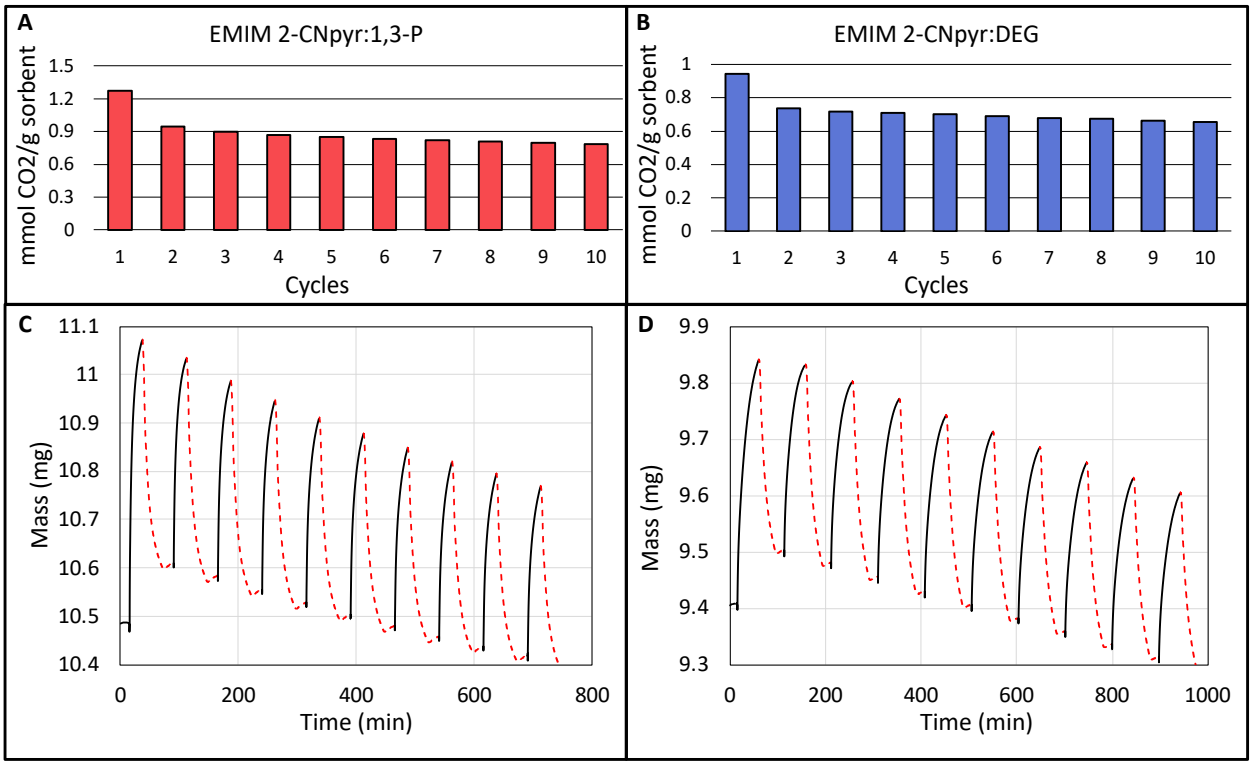

Figure 4. CO_2 sorption and desorption experiments conducted using TGA. [EMIM][2-CNpyr]:1,3-P results showed A) the CO_2 capacity per cycle (red bar graph) and C) the sorption/desorption curves based on mass where the absorption (solid black) is under a pure CO_2 environment at 25 °C and desorption (dashed red) is under a N_2 environment at 55 °C. [EMIM][2-CNpyr]:DEG results are outlined by B) the CO_2 capacity per cycle (blue bar graph) and D) the sorption/desorption curves based on mass with the same conditions as C.

Breakthrough Experiments. To access the sorbent performance of [EMIM][2-CNpyr], [EMIM][2-CNpyr]:DEG, and [EMIM][2-CNpyr]:1,3-P capsules and rate limitations (e.g., diffusion and reaction kinetics), breakthrough analyses were conducted. In a typical breakthrough experiment, capsules were packed in a column such that gas could be flowed through and the concentration of CO_2 coming out of the column measured. An ideal sorbent, i.e., one with no rate limitations, will present a step curve, where all CO_2 in the gas stream is absorbed until the sorbent reaches saturation, at which point the CO_2 concentration in the effluent will increase to the feed concentration. The breakthrough time (t_{BT}) is determined when the effluent concentration reaches 5 % of the feed concentration (25 ppm CO_2). Sorbents with greater mass transport limitations will present elongated S-curves, where elongation increases with greater kinetic barriers.

All three capsule types showed rate limitations such that by integrating the curves with respect to the feed concentration from 0 min to t_{BT} and t_{PE}, the breakthrough capacity and the pseudoequilibrium capacity, respectively, can be determined. The first 200 minutes of breakthrough curves for capsules of [EMIM][2-CNpyr], [EMIM][2-CNpyr]:DEG, and [EMIM][2-CNpyr]:1,3-P at 500 ppm CO_2 are presented in **Figure 5A**. The CO_2 loading over time is plotted in **Figure 5B**. Capsules containing only [EMIM][2-CNpyr] in the core were severely rate limited and did not absorb all CO_2 in the feed at the start of the experiment. This may be due to the low core loading (25 ± 1.8 wt%), however, this was comparable to the [EMIM][2-CNpyr]:1,3-P (28 ±

1.6 wt%) and [EMIM][2-CNpyr]:DEG (34 ± 3.6 wt%). Another possible cause for the limited breakthrough time could be column packing, as these capsules were highly aggregated and sticky compared to the [EMIM][2-CNpyr]:DEG and [EMIM][2-CNpyr]:1,3-P capsules, which made it very difficult to create a uniformly packed column without breaking the capsules. Aggregation also yields larger effective particles, significantly increasing diffusion distance and leading to greater rate limitations. The higher viscosity of the pure [EMIM][2-CNpyr] (75.3 ±2.1 cP) compared to the glycol mixtures of [EMIM][2-CNpyr]:1,3-P (51.1 ± 2.1 cP) and [EMIM][2-CNpyr]:DEG (55.8 ± 2.4 cP) is also likely a significant factor impacting the sorption rate, especially in combination with capsule aggregation. The ratio of CO_2 to [EMIM][2-CNpyr] at full capacity is consistent with isotherm sorption values for bulk [EMIM][2-CNpyr] at 50 Pa (~500 ppm).[14] Capsules containing [EMIM][2-CNpyr]:1,3-P mixture had a t_{BT} of 44 minutes, indicating significantly reduced kinetic limitations compared the capsules of pure IL. These capsules were also a much finer powder which made uniform packing feasible. The pseudoequilibrium capacity was much higher as well, which is consistent with previous reports in a mixture of [EMIM][2-CNpyr] with EG, where the ratio of CO_2 to [EMIM][2-CNpyr] at lower partial pressures dramatically increases upon mixing with a hydrogen bond donor due to an additional "carbonate" binding route, where the hydroxyl is deprotonated by the highly basic IL anion as reported by Lee et al.[19]

Interestingly, the capsules containing [EMIM][2-CNpyr]:DEG in the core had a lower breakthrough time, 19 minutes, as well as a lower time to pseudoequilibrium, and yet displayed a much higher pseudoequilibrium capacity compared to the [EMIM][2-CNpyr]:1,3-P capsules. This is likely due to the [EMIM][2-CNpyr]:1,3-P capsules losing some 1,3-P over the extended sorption cycle, reducing the impact of the aforementioned carbonate formation and increasing the diffusion resistance for CO_2 by increasing viscosity. This is not observed to the same extent in the [EMIM][2-CNpyr]:DEG due to the higher boiling point of DEG, leading to greater overall CO_2 capacity of the mixture at low partial pressure, despite greater diffusion limitations. Both capsules were observed to be fine powders and were easily packed into the column, and thus the packing density was assumed to be similar.

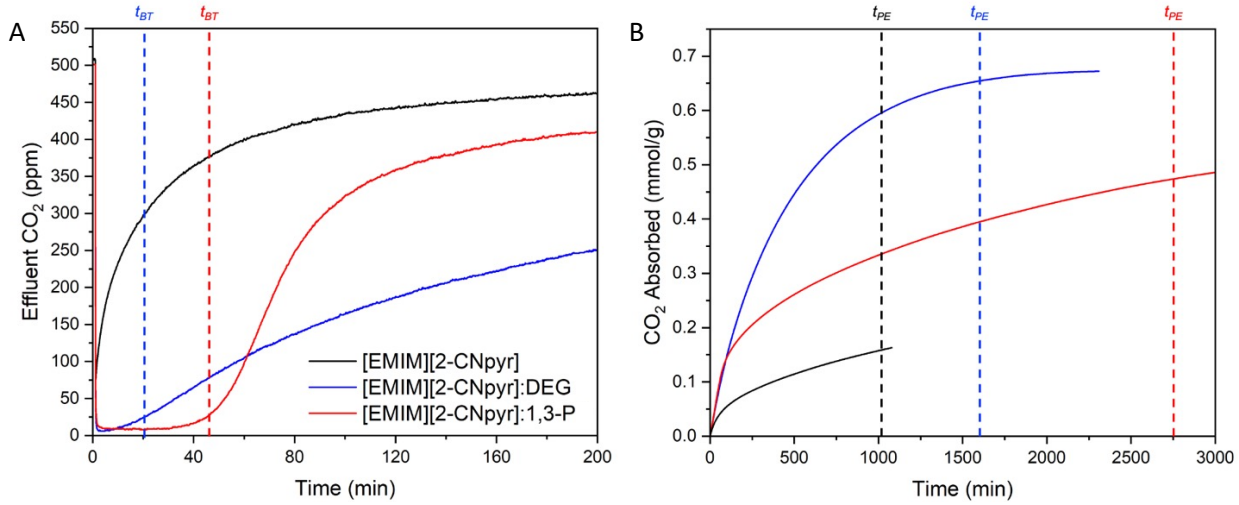

Figure 5. Results of breakthrough experiments for capsules with [EMIM][2-CNpyr]-based cores. (A) First 200 minutes of breakthrough curves, with vertical dashed lines signifying the breakthrough time for each capsule. (B) CO_2 loading of the capsules calculated from the effluent CO_2 concentration using **Eq. 2**. Vertical dashed lines signify the pseudoequilibrium time.

By using the measured capsule composition, the ratio of CO_2 to [EMIM][2-CNpyr] could be determined, which represents the binding site saturation of the [EMIM][2-CNpyr] in the capsules. These values are presented in **Table 2**. Capsules of pure [EMIM][2-CNpyr] had a breakthrough CO_2 capacity of 0 due to significant kinetic barriers and packing limitations, in which the measured effluent CO_2 concentration never reached 25 ppm. In contrast, capsules of [EMIM][2-CNpyr]:1,3-P had the largest breakthrough CO_2 capacity (0.08 mol CO_2/kg sorbent), despite having the longest pseudoequilibrium time (2756 min). [EMIM][2-CNpyr]:DEG capsules had a lower breakthrough CO_2 capacity of 0.03 mol CO_2/kg sorbent with almost half the pseudoequilibrium time (1637 min) compared to [EMIM][2-CNpyr]:1,3-P capsules. Interestingly, [EMIM][2-CNpyr]:DEG had the highest pseudoequilibrium CO_2 capacity (0.66 mol CO_2/kg sorbent), which suggests a higher binding site saturation ratio of 0.75. Although the core loading wt% is lower with capsules of pure [EMIM][2-CNpyr] compared to the capsules of the mixtures, pure [EMIM][2-CNpyr] capsules and [EMIM][2-CNpyr]:1,3-P capsules had similar core loading wt% (25 ± 1.8 and 28 ± 1.6 wt%, respectively), yet the pseudoequilibrium CO_2 capacity was much higher for [EMIM][2-CNpyr]:1,3-P.

Table 2. CO_2 absorption times and capacities under 500 ppm CO_2 in dry N_2.

Capsule core	**Breakthrough CO_2 capacity** (mol CO_2/kg sorbent)	**Pseudoequilibrium time** (min)	**Pseudoequilibrium CO_2 capacity** (mol CO_2 / kg sorbent)	**Binding site saturation (CO_2:IL)**	**Core loading wt%**
[EMIM][2-CNpyr]	0	1027	0.16	0.13	25 ± 1.8
[EMIM][2-CNpyr]:1,3-P	0.08	2756	0.47	0.35	28 ± 1.6
[EMIM][2-CNpyr]:DEG	0.03	1637	0.66	0.75	34 ± 3.6

Conclusions

The use of glycols as a viscosity modifier for IL-based mixtures for CO_2 sorption successfully decreased the viscosity and evaporation rates, however, there was a noticeable interaction between the glycol and a task-specific IL (TSILs) (i.e., [EMIM][2-CNpyr]). The decrease in evaporation is mainly attributed to the diffusion limitations of the glycols through the IL and molecular interactions (e.g., hydrogen bonding, etc.). To further decrease the evaporation rate of the mixtures, microencapsulation via a soft-templated approach was utilized. Encapsulated pure glycols and IL:glycol mixtures demonstrated the ability of the polyurea shell to act as a barrier while also increasing the working surface area of the sorbents. The two lowest evaporation rate mixtures were used for CO_2 sorption with [EMIM][2-CNpyr] were DEG and 1,3-P. It was found that the capsules of [EMIM][2-CNpyr]:DEG had the highest CO_2 capacity, albeit with a large kinetic barrier as determined by sorption/desorption cycles and breakthrough experiments. The use of ILs for sorption requirements can be utilized to a greater effect with the use of viscosity modifiers and encapsulation.

Author Information

Corresponding Authors

Burcu Gurkan – *Department of Chemical and Biomolecular Engineering, Case Western Reserve University, Cleveland, Ohio 44106, Unites States;* Email: beg23@case.edu

Emily B. Pentzer – *Department of Materials Science & Engineering, Texas A&M University, 3003 TAMU; College Station, TX 77843 (USA); Department of Chemistry, Texas A&M University, College Station, Texas 77843, USA;* Email: emilypentzer@tamu.edu

Authors

Cameron D.L. Taylor – *Department of Materials Science & Engineering, Texas A&M University, 3003 TAMU; College Station, TX 77843 (USA)*

Aidan Klemm – *Department of Chemical and Biomolecular Engineering, Case Western Reserve University, Cleveland, Ohio 44106, Unites States*

Luma Al-Mahbobi – *Department of Materials Science & Engineering, Texas A&M University, 3003 TAMU; College Station, TX 77843 (USA)*

B. Jack Bradford – *Department of Materials Science & Engineering, Texas A&M University, 3003 TAMU; College Station, TX 77843 (USA)*

Acknowledgments

This material is based upon work supported by the U.S. Department of Energy under Award No. DE-SC0022214.

Abbreviations

DAC = direct air capture

IL = ionic liquid

TSIL = task specific ionic liquid

EG = ethylene glycol

1,3-P = 1,3-propanediol

PG = propylene glycol

DEG = diethylene glycol

[EMIM][2-CNpyr] = 1-ethyl-3-methylimidazolium 2-cyanopyrrolide

[BMIM][BF4] = 1-butyl-3-methylimidazolium tetrafluoroborate

[EMIM][BF4] = 1-Ethyl-3-methylimidazolium tetrafluoroborate

DAPM = 4,4′-diaminodiphenylmethane

HDI = hexamethylene diisocyanate

GO = graphene oxide

TGA = thermogravimetric analysis

References

(1) Summary for Policymakers. In *Climate Change 2021 – The Physical Science Basis*; Cambridge University Press, 2023; pp 3–32. https://doi.org/10.1017/9781009157896.001.

(2) Ingvarsdóttir, A. *Comparison of Direct Air Capture Technology to Point Source CO2 Capture in Iceland*; Stockholm, 2020.

(3) Custelcean, R. Direct Air Capture of CO2 Using Solvents. *Annu Rev Chem Biomol Eng* **2022**, *13*, 217–234. https://doi.org/10.1146/annurev-chembioeng.

(4) Shi, X.; Lin, Y.; Chen, X. Development of Sorbent Materials for Direct Air Capture of CO2. *MRS Bulletin*. Springer Nature April 1, 2022, pp 405–415. https://doi.org/10.1557/s43577-022-00320-7.

(5) Fujikawa, S.; Selyanchyn, R. Direct Air Capture by Membranes. *MRS Bulletin*. Springer Nature April 1, 2022, pp 416–423. https://doi.org/10.1557/s43577-022-00313-6.

(6) McQueen, N.; Gomes, K. V.; McCormick, C.; Blumanthal, K.; Pisciotta, M.; Wilcox, J. A Review of Direct Air Capture (DAC): Scaling up Commercial Technologies and Innovating for the Future. *Progress in Energy*. Institute of Physics July 1, 2021. https://doi.org/10.1088/2516-1083/abf1ce.

(7) Recker, E. A.; Green, M.; Soltani, M.; Paull, D. H.; Mcmanus, G. J.; Davis, J. H.; Mirjafari, A. Direct Air Capture of CO2via Ionic Liquids Derived from “Waste” Amino

Acids. *ACS Sustain Chem Eng* **2022**, *10* (36), 11885–11890. https://doi.org/10.1021/acssuschemeng.2c02883.
(8) Shannon, M. S.; Tedstone, J. M.; Danielsen, S. P. O.; Hindman, M. S.; Irvin, A. C.; Bara, J. E. Free Volume as the Basis of Gas Solubility and Selectivity in Imidazolium-Based Ionic Liquids. *Ind Eng Chem Res* **2012**, *51* (15), 5565–5576. https://doi.org/10.1021/ie202916e.
(9) Jeffrey Horne, W.; Shannon, M. S.; Bara, J. E. Correlating Fractional Free Volume to CO2 Selectivity in [Rmim][Tf2N] Ionic Liquids. *Journal of Chemical Thermodynamics* **2014**, *77*, 190–196. https://doi.org/10.1016/j.jct.2014.03.012.
(10) Bates, E. D.; Mayton, R. D.; Ntai, I.; Davis, J. H. CO2 Capture by a Task-Specific Ionic Liquid. *J Am Chem Soc* **2002**, *124* (6), 926–927. https://doi.org/10.1021/ja017593d.
(11) Shi, C.; Quiroz-Guzman, M.; DeSilva, A.; Brennecke, J. F. Physicochemical and Electrochemical Properties of Novel Ionic Liquids Containing Aprotic Heterocyclic Anions Doped with Lithium Salts. *ECS Trans* **2013**, *50* (11), 309–324. https://doi.org/10.1149/05011.0309ecst.
(12) Brown, P.; Gurkan, B. E.; Hatton, T. A. Enhanced Gravimetric CO2 Capacity and Viscosity for Ionic Liquids with Cyanopyrrolide Anion. *AIChE Journal* **2015**, *61* (7), 2280–2285. https://doi.org/10.1002/aic.14819.
(13) Lee, Y. Y.; Gurkan, B. Graphene Oxide Reinforced Facilitated Transport Membrane with Poly(Ionic Liquid) and Ionic Liquid Carriers for CO2/N2 Separation. *J Memb Sci* **2021**, *638*. https://doi.org/10.1016/j.memsci.2021.119652.
(14) Lee, Y. Y.; Edgehouse, K.; Klemm, A.; Mao, H.; Pentzer, E.; Gurkan, B. Capsules of Reactive Ionic Liquids for Selective Capture of Carbon Dioxide at Low Concentrations. *ACS Appl Mater Interfaces* **2020**, *12* (16), 19184–19193. https://doi.org/10.1021/acsami.0c01622.
(15) Qu, Y.; Zhao, Y.; Li, D.; Sun, J. Task-Specific Ionic Liquids for Carbon Dioxide Absorption and Conversion into Value-Added Products. *Curr Opin Green Sustain Chem* **2022**, *34*, 100599. https://doi.org/10.1016/J.COGSC.2022.100599.
(16) Mota-Martinez, M. T.; Brandl, P.; Hallett, J. P.; Mac Dowell, N. Challenges and Opportunities for the Utilisation of Ionic Liquids as Solvents for CO2 Capture. *Mol Syst Des Eng* **2018**, *3* (3), 560–571. https://doi.org/10.1039/c8me00009c.
(17) Gutowski, K. E.; Maginn, E. J. Amine-Functionalized Task-Specific Ionic Liquids: A Mechanistic Explanation for the Dramatic Increase in Viscosity upon Complexation with CO2 from Molecular Simulation. *J Am Chem Soc* **2008**, *130* (44), 14690–14704. https://doi.org/10.1021/ja804654b.
(18) Yang, J.; Yu, X.; Yan, J.; Tu, S. T. CO2 Capture Using Amine Solution Mixed with Ionic Liquid. *Ind Eng Chem Res* **2014**, *53* (7), 2790–2799. https://doi.org/10.1021/ie4040658.
(19) Lee, Y. Y.; Penley, D.; Klemm, A.; Dean, W.; Gurkan, B. Deep Eutectic Solvent Formed by Imidazolium Cyanopyrrolide and Ethylene Glycol for Reactive CO2Separations. *ACS Sustain Chem Eng* **2021**, *9* (3), 1090–1098. https://doi.org/10.1021/acssuschemeng.0c07217.
(20) Camper, D.; Bara, J. E.; Gin, D. L.; Noble, R. D. Room-Temperature Ionic Liquid-Amine Solutions: Tunable Solvents for Efficient and Reversible Capture of CO2. *Ind Eng Chem Res* **2008**, *47* (21), 8496–8498. https://doi.org/10.1021/ie801002m.
(21) Nookuea, W.; Wang, F.; Yang, J.; Tan, Y.; Li, H.; Thorin, E.; Yu, X.; Yan, J. Viscosity Data of Aqueous MDEA-[Bmim][BF4] Solutions Within Carbon Capture Operating

Conditions. In *Energy Procedia*; Elsevier Ltd, 2017; Vol. 105, pp 4581–4586. https://doi.org/10.1016/j.egypro.2017.03.987.

(22) Wang, Z.; Wang, Z.; Huang, X.; Yang, D.; Wu, C.; Chen, J. Deep Eutectic Solvents Composed of Bio-Phenol-Derived Superbase Ionic Liquids and Ethylene Glycol for CO2 Capture. *Chemical Communications* **2022**, *58* (13), 2160–2163. https://doi.org/10.1039/d1cc06856c.

(23) Gao, H.; Bai, L.; Han, J.; Yang, B.; Zhang, S.; Zhang, X. Functionalized Ionic Liquid Membranes for CO2 Separation. *Chemical Communications* **2018**, *54* (90), 12671–12685. https://doi.org/10.1039/c8cc07348a.

(24) Friess, K.; Izák, P.; Kárászová, M.; Pasichnyk, M.; Lanč, M.; Nikolaeva, D.; Luis, P.; Jansen, J. C. A Review on Ionic Liquid Gas Separation Membranes. *Membranes*. MDPI AG February 1, 2021, pp 1–58. https://doi.org/10.3390/membranes11020097.

(25) Fu, Y.; Yang, Z.; Mahurin, S. M.; Dai, S.; Jiang, D. en. Ionic Liquids for Carbon Capture. *MRS Bulletin*. Springer Nature April 1, 2022, pp 395–404. https://doi.org/10.1557/s43577-022-00315-4.

(26) Wang, Z.; Wang, Y.; Chen, J.; Arnould, M.; Popovs, I.; Mahurin, S. M.; Chen, H.; Wang, T.; Dai, S. Synthesis of Poly(Ionic Liquid)s- Block-Poly(Methyl Methacrylate) Copolymer-Grafted Silica Particle Brushes with Enhanced CO2Permeability and Mechanical Performance. *Langmuir* **2021**, *37* (36), 10875–10881. https://doi.org/10.1021/acs.langmuir.1c01877.

(27) Yao, J.; Sheng, M.; Bai, S.; Su, H.; Shang, H.; Deng, H.; Sun, J. Ionic Liquids Grafted Mesoporous Silica for Chemical Fixation of CO2 to Cyclic Carbonate: Morphology Effect. *Catal Letters* **2022**, *152* (3), 781–790. https://doi.org/10.1007/s10562-021-03667-9.

(28) Zhu, J.; He, B.; Huang, J.; Li, C.; Ren, T. Effect of Immobilization Methods and the Pore Structure on CO2 Separation Performance in Silica-Supported Ionic Liquids. *Microporous and Mesoporous Materials* **2018**, *260*, 190–200. https://doi.org/10.1016/j.micromeso.2017.10.035.

(29) Uehara, Y.; Karami, D.; Mahinpey, N. Roles of Cation and Anion of Amino Acid Anion-Functionalized Ionic Liquids Immobilized into a Porous Support for CO2 Capture. *Energy and Fuels* **2018**, *32* (4), 5345–5354. https://doi.org/10.1021/acs.energyfuels.8b00190.

(30) Wang, H.; Zhu, J.; Tan, L.; Zhou, M.; Zhang, S. Encapsulated Ionic Liquids for CO2 Capture. *Mater Chem Phys* **2020**, *251*. https://doi.org/10.1016/j.matchemphys.2020.122982.

(31) Santiago, R.; Lemus, J.; Moya, C.; Moreno, D.; Alonso-Morales, N.; Palomar, J. Encapsulated Ionic Liquids to Enable the Practical Application of Amino Acid-Based Ionic Liquids in CO2 Capture. *ACS Sustain Chem Eng* **2018**, *6* (11), 14178–14187. https://doi.org/10.1021/acssuschemeng.8b02797.

(32) Starvaggi, N. C.; Bradford, B. J.; Taylor, C. D. L.; Pentzer, E. B. Wettability-Tuned Silica Particles for Emulsion-Templated Microcapsules. *Soft Matter* **2023**, *19* (39), 7635–7643. https://doi.org/10.1039/d3sm00860f.

(33) Hussain Solangi, N.; Hussin, F.; Anjum, A.; Sabzoi, N.; Ali Mazari, S.; Mubarak, N. M.; Kheireddine Aroua, M.; Siddiqui, M. T. H.; Saeed Qureshi, S. A Review of Encapsulated Ionic Liquids for CO2 Capture. *Journal of Molecular Liquids*. Elsevier B.V. March 15, 2023. https://doi.org/10.1016/j.molliq.2023.121266.

(34) Song, T.; Avelar Bonilla, G. M.; Morales-Collazo, O.; Lubben, M. J.; Brennecke, J. F. Recyclability of Encapsulated Ionic Liquids for Post-Combustion CO2 Capture. *Ind Eng Chem Res* **2019**, *58* (12), 4997–5007. https://doi.org/10.1021/acs.iecr.9b00251.
(35) Gaur, S. S.; Edgehouse, K. J.; Klemm, A.; Wei, P.; Gurkan, B.; Pentzer, E. B. Capsules with Polyurea Shells and Ionic Liquid Cores for CO2 Capture. *Journal of Polymer Science* **2021**, *59* (23), 2980–2989. https://doi.org/10.1002/pol.20210342.
(36) Knipe, J. M.; Chavez, K. P.; Hornbostel, K. M.; Worthington, M. A.; Nguyen, D. T.; Ye, C.; Bourcier, W. L.; Baker, S. E.; Brennecke, J. F.; Stolaroff, J. K. Evaluating the Performance of Micro-Encapsulated CO2 Sorbents during CO2 Absorption and Regeneration Cycling. *Environ Sci Technol* **2019**, *53* (5), 2926–2936. https://doi.org/10.1021/acs.est.8b06442.
(37) Silva, L. P.; Moya, C.; Sousa, M.; Santiago, R.; Sintra, T. E.; Carreira, A. R. F.; Palomar, J.; Coutinho, J. A. P.; Carvalho, P. J. Encapsulated Amino-Acid-Based Ionic Liquids for CO2 Capture. *Eur J Inorg Chem* **2020**, *2020* (33), 3158–3166. https://doi.org/10.1002/ejic.202000364.
(38) Bernard, F. L.; Duarte, E. A.; Polesso, B. B.; Duczinski, R. B.; Einloft, S. CO2 Sorption Using Encapsulated Imidazolium-Based Fluorinated Ionic Liquids. *Environmental Challenges* **2021**, *4*. https://doi.org/10.1016/j.envc.2021.100109.
(39) Luo, Q.; Wang, Y.; Yoo, E.; Wei, P.; Pentzer, E. Ionic Liquid-Containing Pickering Emulsions Stabilized by Graphene Oxide-Based Surfactants. *Langmuir* **2018**, *34* (34), 10114–10122. https://doi.org/10.1021/acs.langmuir.8b02011.
(40) Luo, Q.; Wang, Y.; Chen, Z.; Wei, P.; Yoo, E.; Pentzer, E. Pickering Emulsion-Templated Encapsulation of Ionic Liquids for Contaminant Removal. *ACS Appl Mater Interfaces* **2019**, *11* (9), 9612–9620. https://doi.org/10.1021/acsami.8b21881.
(41) Luo, Q.; Pentzer, E. Encapsulation of Ionic Liquids for Tailored Applications. *ACS Appl Mater Interfaces* **2020**, *12* (5), 5169–5176. https://doi.org/10.1021/acsami.9b16546.
(42) Edgehouse, K. J.; Rosenfeld, N.; Bergbreiter, D. E.; Pentzer, E. B. Capsules of the Poly(α-Olefin) PAO432for Removal of BTEX Contaminants from Water. *Ind Eng Chem Res* **2021**, *60* (40), 14455–14463. https://doi.org/10.1021/acs.iecr.1c02819.
(43) Edgehouse, K.; Starvaggi, N.; Rosenfeld, N.; Bergbreiter, D.; Pentzer, E. Impact of Shell Composition on Dye Uptake by Capsules of Ionic Liquid. *Langmuir* **2022**, *38* (45), 13849–13856. https://doi.org/10.1021/acs.langmuir.2c02015.
(44) Baca, K. R.; Harders, A. N.; Starvaggi, N.; Yancey, A. D.; Wang, Y.; Pentzer, E.; Shiflett, M. B. First Measurements of the Sorption of Difluoromethane and Pentafluoroethane in Encapsulated Ionic Liquids. *Ind Eng Chem Res* **2023**, *62* (36), 14522–14536. https://doi.org/10.1021/acs.iecr.3c01745.
(45) Gaur, S. S.; Edgehouse, K. J.; Klemm, A.; Wei, P.; Gurkan, B.; Pentzer, E. B. Capsules with Polyurea Shells and Ionic Liquid Cores for CO2 Capture. *Journal of Polymer Science* **2021**, *59* (23), 2980–2989. https://doi.org/10.1002/pol.20210342.
(46) Huang, Q.; Luo, Q.; Wang, Y.; Pentzer, E.; Gurkan, B. Hybrid Ionic Liquid Capsules for Rapid CO 2 Capture . *Ind Eng Chem Res* **2019**, *58* (24), 10503–10509. https://doi.org/10.1021/acs.iecr.9b00314.
(47) Lak, S. N.; Ahmed, S.; Shamberger, P. J.; Pentzer, E. B. Encapsulation of Hygroscopic Liquids via Polymer Precipitation in Non-Aqueous Emulsions. *J Colloid Interface Sci* **2022**, *628*, 605–613. https://doi.org/10.1016/j.jcis.2022.08.083.

(48) Wang, Y.; Starvaggi, N.; Pentzer, E. Capsules with Responsive Polymeric Shells for Applications beyond Drug Delivery. *Polymer Chemistry*. Royal Society of Chemistry August 25, 2023, pp 4033–4047. https://doi.org/10.1039/d3py00434a.
(49) Wang, Y.; Wei, P.; Zhou, Q.; Cipriani, C.; Qi, M.; Sukhishvili, S.; Pentzer, E. Temperature-Dependent Capsule Shell Bonding and Destruction Based on Hindered Poly(Urea-Urethane) Chemistry. *Chemistry of Materials* **2022**, *34* (13), 5821–5831. https://doi.org/10.1021/acs.chemmater.2c00415.
(50) Wang, Y.; Quevedo, K.; Pentzer, E. Inter-Capsule Fusion and Capsule Shell Destruction Using Dynamic Covalent Polymers. *Polym Chem* **2021**, *12* (18), 2695–2700. https://doi.org/10.1039/d1py00271f.
(51) Dikki, R.; Cagli, E.; Penley, D.; Karayilan, M.; Gurkan, B. Formation of Choline Salts and Dipolar Ions for CO2 Reactive Eutectic Solvents. *Chemical Communications* **2023**, *59* (80), 12027–12030. https://doi.org/10.1039/d3cc03272h.
(52) Klemm, A.; Vicchio, S. P.; Bhattacharjee, S.; Cagli, E.; Park, Y.; Zeeshan, M.; Dikki, R.; Liu, H.; Kidder, M. K.; Getman, R. B.; Gurkan, B. Impact of Hydrogen Bonds on CO2 Binding in Eutectic Solvents: An Experimental and Computational Study toward Sorbent Design for CO2 Capture. *ACS Sustain Chem Eng* **2023**, *11* (9), 3740–3749. https://doi.org/10.1021/acssuschemeng.2c06767.
(53) Yaghini, N.; Abdurrokhman, I.; Hasani, M.; Martinelli, A. Transport Properties and Intermolecular Interactions in Binary Mixtures Based on the Protic Ionic Liquid Ethylimidazolium Triflate and Ethylene Glycol. *Physical Chemistry Chemical Physics* **2018**, *20* (35), 22980–22986. https://doi.org/10.1039/c8cp03093f.
(54) Kumar, B.; Singh, T.; Rao, K. S.; Pal, A.; Kumar, A. Thermodynamic and Spectroscopic Studies on Binary Mixtures of Imidazolium Ionic Liquids in Ethylene Glycol. *Journal of Chemical Thermodynamics* **2012**, *44* (1), 121–127. https://doi.org/10.1016/j.jct.2011.08.008.
(55) Ibrahim, R. K.; Hayyan, M.; Alsaadi, M. A.; Ibrahim, S.; Hayyan, A.; Hashim, M. A. Diethylene Glycol Based Deep Eutectic Solvents and Their Physical Properties. *Studia Universitatis Babes-Bolyai Chemia* **2017**, *62* (4), 433–450. https://doi.org/10.24193/subbchem.2017.4.37.
(56) Latnikova, A.; Jobmann, M. Towards Microcapsules with Improved Barrier Properties. https://doi.org/10.1007/s41061-017-0152.
(57) Dimiev, A.; Kosynkin, D. V.; Alemany, L. B.; Chaguine, P.; Tour, J. M. Pristine Graphite Oxide. *J Am Chem Soc* **2012**, *134* (5), 2815–2822. https://doi.org/10.1021/ja211531y.
(58) Kortunov, P. V.; Baugh, L. S.; Siskin, M. Pathways of the Chemical Reaction of Carbon Dioxide with Ionic Liquids and Amines in Ionic Liquid Solution. *Energy and Fuels* **2015**, *29* (9), 5990–6007. https://doi.org/10.1021/acs.energyfuels.5b00876.
(59) Seo, S.; Desilva, M. A.; Brennecke, J. F. Physical Properties and CO2 Reaction Pathway of 1-Ethyl-3-Methylimidazolium Ionic Liquids with Aprotic Heterocyclic Anions. *Journal of Physical Chemistry B* **2014**, *118* (51), 14870–14879. https://doi.org/10.1021/jp509583c.
(60) Lee, Y. Y.; Cagli, E.; Klemm, A.; Park, Y.; Dikki, R.; Kidder, M. K.; Gurkan, B. Microwave Regeneration and Thermal and Oxidative Stability of Imidazolium Cyanopyrrolide Ionic Liquid for Direct Air Capture of Carbon Dioxide. *ChemSusChem* **2023**, *16* (13). https://doi.org/10.1002/cssc.202300118.
(61) Rafiee, H. R.; Frouzesh, F. The Study of Partial and Excess Molar Volumes for Binary Mixtures of Nitrobenzene and Benzaldehyde with Xylene Isomers from T = (298.15 to

318.15) K and P = 0.087 MPa. *J Adv Res* **2016**, *7* (5), 769–780. https://doi.org/10.1016/j.jare.2015.11.003.
(62) Chen, Y.; Han, X.; Liu, Z.; Li, Y.; Sun, H.; Wang, H.; Wang, J. Thermal Decomposition and Volatility of Ionic Liquids: Factors, Evaluation and Strategies. *Journal of Molecular Liquids*. Elsevier B.V. November 15, 2022. https://doi.org/10.1016/j.molliq.2022.120336.
(63) Lide, D. R.; Kehiaian, H. V. *CRC HANDBOOK of THERMOPHYSICAL and THERMOCHEMICAL DATA*, 1st ed.; CRC Press: Boca Raton, 1994. https://doi.org/10.1201/9781003067719.
(64) George, J.; Sastry, N. V. Densities, Dynamic Viscosities, Speeds of Sound, and Relative Permittivities for Water + Alkanediols (Propane-1,2- and -1,3-Diol and Butane-1,2-, -1,3-, -1,4-, and -2,3-Diol) at Different Temperatures. *J Chem Eng Data* **2003**, *48* (6), 1529–1539. https://doi.org/10.1021/je0340755.
(65) Budeanu, M. M.; Dumitrescu, V. Densities, Viscosities and Excess Properties for Dimethyl Sulfoxide with Diethylene Glycol and Methyldiethanolamine at Different Temperatures. *Applied Sciences (Switzerland)* **2022**, *12* (1). https://doi.org/10.3390/app12010116.
(66) Dai, Y.; Qu, Y.; Wang, S.; Wang, J. Measurement, Correlation, and Prediction of Vapor Pressure for Binary and Ternary Systems Containing an Ionic Liquid 1,3-Dimethylimidazolium Methylsulfate. *Fluid Phase Equilib* **2015**, *385*, 219–226. https://doi.org/10.1016/j.fluid.2014.10.028.